BioChip Journal (2022) 16:58–66
https://doi.org/10.1007/s13206-022-00046-3

ORIGINAL ARTICLE

Homobifunctional Imidoester Combined Black Phosphorus Nanosheets Used as Cofactors for Nucleic Acid Extraction

Huifang Liu[1] · Qingshuang Zou[1] · Myoung Gyu Kim[1,2] · Zhen Qiao[1] · Dao Thi Thuy Nguyen[1] · Bonhan Koo[1] · Hyo Joo Lee[1] · Yoon Ok Jang[1] · Jun Ki Kim[2] · Yong Shin[1]

Received: 3 November 2021 / Revised: 19 January 2022 / Accepted: 21 January 2022 / Published online: 7 February 2022

Abstract
Studies on nucleic acid-based diagnostics technology have been widely applied to clinical disease diagnosis. In particular, practical effective techniques for the isolation and purification of nucleic acids from pathogenic cells are crucial to ensure the accuracy of analysis. However, numerous organic reagents from the current commercial nucleic acid extraction kits have varied potential side effects in early and further specific diagnosis. Here, we present an easy-to-operate assay for nucleic acid extraction through an outstanding two-dimensional material—black phosphorus (BP), which has attracted significant interest in the diagnosis and treatment of diseases due to its high charge carrier mobility, strong optical absorption, and excellent bioactivity. With the characterization of BP, we proposed an optimized nucleic acid extraction system. A portable-safe single 808 nm near-infrared (NIR) laser was used for the BP thermal heating system for nucleic acid extraction without any larger thermal instrument. We found that the purity and quantity of nucleic acid extracted in the BP-based system were three times higher than in a commercial kit. We also modified the nanosized BP coated with homobifunctional imidoester (HI) to enhance the biomolecule binding with both biocompatibility and surface-crosslinking abilities. We believe that the BP-HI-laser system could be a good candidate for designing nucleic acid extraction for disease diagnosis systems.

Keywords Nucleic acid extraction · Black phosphorus · Homobifunctional imidoesters · Disease diagnosis system · Molecular diagnostics

1 Introduction

Currently, medical and health services globally face major challenges regarding pathogen infection [1–3]; their quick and accurate detection remains a major topic of scientific research [4, 5]. In particular, different approaches toward DNA extraction have rapidly developed in the last century and have been applied in disease diagnosis [6, 7]. At present, the main methods for DNA extraction are the concentrated salt method, anion decontamination method, water extraction method, phenol extraction method, and enzymatic hydrolysis method [7, 8]. Moreover, methods of the proteolysis cell membrane and DNA extraction have been developed into commercial kits that are widely used [9], such as QIAGEN, BLOG, and Tiangen kits. Today, DNA extraction is considered a reasonably routine process [10]; however, these methods possess shortcoming depending on the type of organism and tissue used. Considering the QIAGEN kit as an example, which works on the principle that the enzyme decomposes the cell membrane and associated proteins to release DNA, however, the enzyme simultaneously damages nucleic acids [11, 12]. Additionally, the kit suffers from DNA content loss since it requires a lot of liquid transfer and multiple elution processes. Since DNA quality, integrity, and yield constantly affect the results of

Huifang Liu, Qingshuang Zou and Myoung Gyu Kim have contributed equally to this work.

✉ Jun Ki Kim
kim@amc.seoul.kr

✉ Yong Shin
shinyongno1@yonsei.ac.kr

[1] Department of Biotechnology, College of Life Science and Biotechnology, Yonsei University, 50 Yonsei-ro, Seodaemun-gu, Seoul 03722, South Korea

[2] Department of Convergence Medicine, Asan Institute for Life Sciences, Asan Medical Center, University of Ulsan College of Medicine, 88 Olympicro-43gil, Songpa-gu, Seoul 05505, South Korea

subsequent experiments, it is vital to choose reliable DNA extraction techniques [13, 14].

The ability to amplify low-copy DNA simultaneously makes in vitro PCR one of the most important techniques in molecular biology [14–16]. However, PCR technology has its own series of shortcomings, thus, its reliability is occasionally questioned and debated [13]. First, sufficient DNA content cannot be obtained in the subsequent PCR cycle amplification process if the test sample has inadequate DNA content, which affects the final test result. Second, PCR inhibitors interact with nucleic acids and interfere with DNA polymerase or other thermostable enzymes, thus, directly influencing the reaction [17, 18]. This interaction with nucleic acid binding may alter amplification and lead to the co-purification of inhibitors and DNA. In addition, DNA polymerases can be directly attacked by inhibitors to block or change their enzymatic activity [19].

Initially, some researchers began to examine nanomaterial-assisted PCR (nanoPCR), and subsequently research groups have investigated and understood mechanisms and interactions between nanomaterials and biological systems. Among them, 2D layered materials, such as graphene and boron/carbon nitride, have attracted enormous interest due to their extraordinary physical and chemical properties and have been developed in the fields of electronics, energy storage, optical modulators, and sensors [20–22]. As a new star of the 2D materials family, black phosphorus (BP) has attracted considerable attention since its first mechanical exfoliation from bulk BP in 2014 [23, 24]. BP consists of corrugated planes of P atoms with strong in-plane covalent bonding and weak interlayer van der Waals interactions, which benefit its bilayer structure along the zigzag direction and puckered lattice configuration along the armchair direction [25, 26]. Thereby, BP is superior due to its much higher surface-to-volume ratios, better molecular adsorption energy, and modified biocompatibility, having wide applications in biochips, drug treatments, nano-bioprobes, and biological applications.

Here, we proposed the use of the photo-thermal properties of BP for the purpose of improving the enzymatic digestion method of a spin-column kit to extract DNA from the pathogen *Escherichia coli* (*E. coli*). As shown in Fig. 1, the BP-near-infrared (NIR)-homobifunctional imidoester (HI) system for DNA extraction was designed based on our optimized nucleic acid protocol [27]. Thereafter, the enriched nucleic acids were simply spun down and eluted using our prepared elution buffer. Nucleic acids released from BP nanosheets were collected, and the quantity and purity of the extracted nucleic acids were checked through RT-PCR and nanodrop to validate the function of the BP-NIR-HI system. Meanwhile, we studied the possible mechanisms of the BP-NIR-HI system through a variable control experiment. As a result, the chemical characterizations (surface potential charge and reactive oxygen species (ROS) release) supported our hypothesis. Furthermore, we proposed a reasonable BP thermal nucleic acid amplification system based on the PCR system. Hopefully, this study on the bioapplication of BP nanosheets will bring about more opportunities relating to the improvement of disease diagnostics for clinical applications.

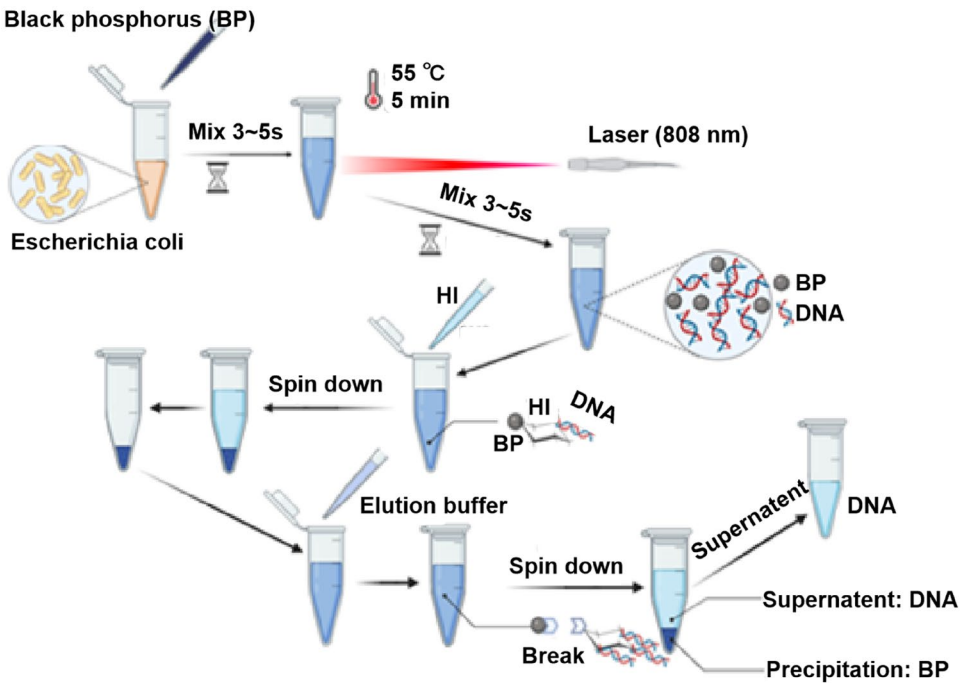

Fig. 1 Flow chart of DNA extraction by the designed black phosphorus-near infrared-homobifunctional imidoester (BP-NIR-HI) system

2 Experiments

2.1 Chemicals and Reagents

All experimental reagents were analytically pure and used without further purification. Dimethyl suberimidate dihydrochloride (DMS; Sigma, 179,523-5G), BP (6 Carbon Technology, Shenzhen), a commercial QIAGEN amp DNA Mini Kit (DNA Mini Kit: Cat No. 51304), Milli-Q water with a resistance greater than 18 MΩ, 99% ethyl alcohol, and phosphate-buffered saline (10×, pH 7.4) were used in all experiments.

2.2 Biological Samples

Prokaryotic *E. coli* (ATCC25922) was inoculated into the nutrient broth or LB (Luria Broth) medium and kept overnight in a shaking incubator at 37 °C and 210 rpm. Samples ranging from 10^3 to 10^5 CFU (Colony-Forming Unit) were used for this study. The primer set was used for enhancing both biocompatibility and surface-crosslinking abilities.

2.3 Preparation of the Black Phosphorus Nanoparticles

BP nanosheets were prepared by bath sonication. Then, 10 mg of the BP mass (multilayer) was dispersed in 10 mL of ultrapure water and treated ultrasonically within an ice bath for 4 h. After sonication, BP nanosheets were collected through centrifugation and dried to a powder in a 56 °C oven for further use. Prepared BP nanosheets were rinsed with alcohol to achieve HI functionalization and enhance both biocompatibility and surface-crosslinking abilities.

2.4 Characterization

An 808 nm laser was used to study the plasmonic thermal effect of BP by irradiation (Beijing Leizhiwei Photoelectric Technology Co., Ltd., China). An infrared imager (E98, FLIR company, Germany) was used to detect the temperature. The field emission scanning electron microscope (FE-SEM) and JSM-7500F (JEOL) were used to characterize the morphology of the BP materials (mass and nanosheet). Energy dispersive x-ray (EDX) analysis was used to analyze the elemental composition in the composite material, and UV/visible spectroscopy was used to determine the composite materials and check the concentration of the BP solution. The stability of materials was tested through zeta potential (Malvern zetasizer). Moreover, the released ROS was detected by a microplate absorbance reader.

2.5 Referred DNA Extraction by QIAZEN kit

First, 200 µL of 1×10^5 *E. coli* sample was mixed with 200 µL of QIAZEN lysis buffer, and 2 µL of proteinase K was then added. Thereafter, this solution was incubated at 55 °C for 10 min. Following this, 200 µL of 100% alcohol was added to the solution, which was then transferred to a filter tube and centrifuged at 8000 rpm for 1 min. After discarding the liquid, 500 µL of AW1 solution was added to the filtered tube, which was then centrifuged at 8000 rpm for 1 min and the liquid was discarded. Next, 500 µL of AW2 solution was added to the filtered tube, centrifuged at 13,000 rpm for 3 min, and the liquid was discarded. Finally, 100 µL of elution was added to the tube. After standing for 1 min, this was then centrifuged at 8000 rpm for 1 min. The resulting solution was the DNA-containing solution.

2.6 Designed BP-NIR-HI System for DNA Extraction

As shown in Fig. 1, the BP-NIR-HI system for DNA extraction was designed based on the optimized nucleic acid protocol. Initially, 200 µL of *E. coli* (*CFU:* 1×10^5) was tested using a commercial kit. First, 200 µL of BP nanosheet was added to the tube and the sample was irradiated by an NIR laser. The irradiation time and current of the laser were adjusted for different concentrations of BP nanosheet solutions to control the thermal system. The goal was to increase the temperature of the system to 55 °C and current to 3 A (ampere) for 2 min of irradiation. The increased temperature of the solution could be maintained for 5 min. To mix the solution well, the tube was vortexed or the bottom of the tube was gently patted. Later, HI (DMS, 50 µL 100 mg/mL) was added to the test tube and mixed for 1 min to help the BP nanosheets extract the nucleic acid. Then, BP nanosheet-based precipitation was obtained by quickly centrifuging at 13,000 rpm for 1 min and removing the supernatant. Finally, 100 µL of elution buffer (pH ~ 10.6) was used to resolve the nucleic acid in the supernatant by pipetting 3–5 times. This was then centrifuged at 13,000 rpm for 1 min to obtain the supernatant, which was the final extracted nucleic acid solution.

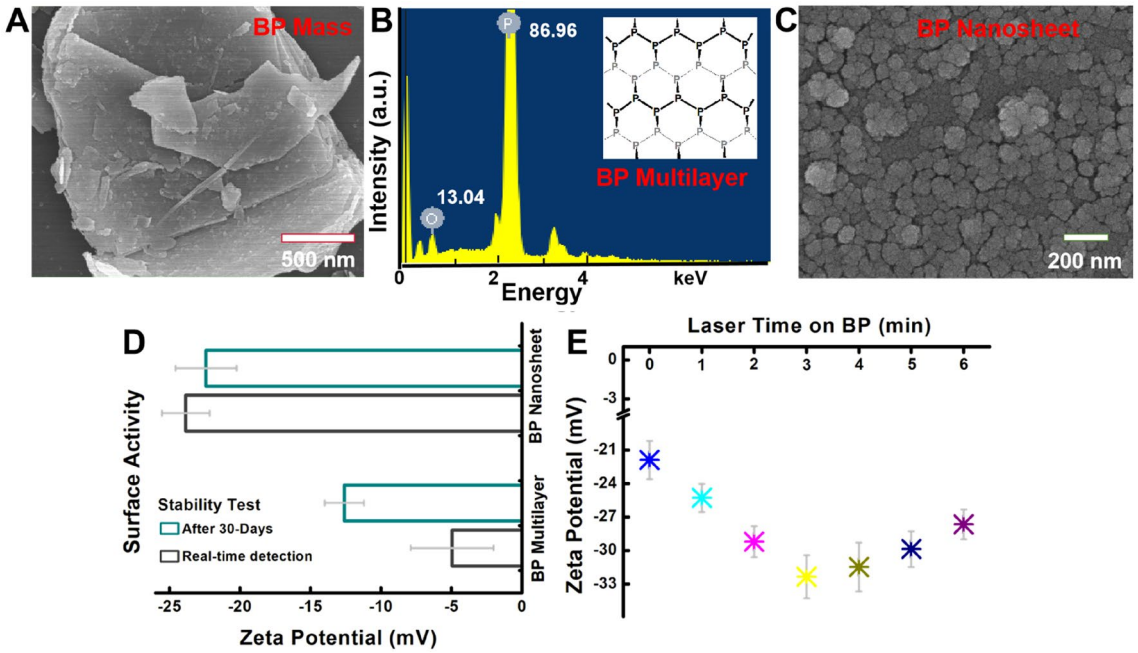

Fig. 2 Characterization of black phosphorous (BP) multilayer and nanosheets after fragmentation. **A** Scanning electron microscope (SEM) image of commercial solid BP. **B** Energy-dispersive X-ray spectroscopy (EDX) spectra of the solid BP and the inside molecular diagram of the BP multilayer. **C** SEM image of BP nanosheets after 4 h in an ultrasonic water bath (size around 50–100 nm). **D** Stability of the BP multilayer and nanosheet through testing the zeta potential value of instant and water-preserved samples. **E** Effect of laser irradiation on the stability of BP nanosheets. Error bars indicate standard deviation from the mean based on at least three independent experiments

3 Results and Discussion

3.1 Characterization of the Black Phosphorous Multilayer and Nanosheets

We proposed a new pathogen DNA extraction strategy (Fig. 1) called the BP-NIR-HI system. First, we analyzed the morphology of the BP materials through SEM. The untreated BP mass showed multilayering with a size of around 3–5 µm (Fig. 2A). According to the assisted EDX spectrum of BP mass shown in Fig. 2B, the high content ratio of P (86.96%) confirmed the properties and purity of the commercial BP mass. Meanwhile, the exited O (13.04%) indicated that the activated surface of BP would be oxidized by the O quickly in the air. After protected sonication, the fragmentation of BP showed dispersion sheets with sizes of less than 100 nm (BP nanosheets, Fig. 2C).

Second, we studied the surface charge of our materials through the zeta potential. We set two factors in one studied group, BP multilayer vs. BP nanosheets, and the stability after maintaining for 30 days (Fig. 2D). We found that the real-time detection of the BP multilayer (surface charge: |– 5|) demonstrated the considerable activity of the BP mass surface [28]. This result also echoes that of the O in the EDX spectrum. Moreover, the surface charge of the BP nanosheets showed that it had less activity than the BP multilayer. We inferred that the oxygenation BP materials were related to the quantity of P. In addition, the BP nanosheets showed higher stability than BP mass in solution. In another studied group, we detected the irradiation time effect on the stability of the BP nanosheets solution. The results (Fig. 2E) showed that the surface charge remained in the range of |±20 ~ ±40|, thus, it was relatively stable.

Third, we studied the laser-plasmonic thermal performances of the BP nanosheets and recorded these using a thermographic imager (Fig. 3A). The current of the laser was optimized through multipoint tests. The timeline of the laser-plasmonic thermal performances of the BP nanosheets (500 µL, within different concentrations, irradiation with current – 2 A for 10 min) was studied using a simple thermometer (Fig. 3B). The pure water was not affected by the laser irradiation. Furthermore, we decreased the amount of solution to 200 µL to obtain an appropriate amount for a further nucleic acid extraction system, and 12 sets are shown in Fig. 3C. The laser irradiation was paused at 10 min to observe the temperature decrease rate. We found that the temperature of the solution could be controlled by adjusting different concentrations of BP nanosheets and different currents of the laser. In addition, the temperature decrease rate after stopping laser irradiation was high-speed. For example,

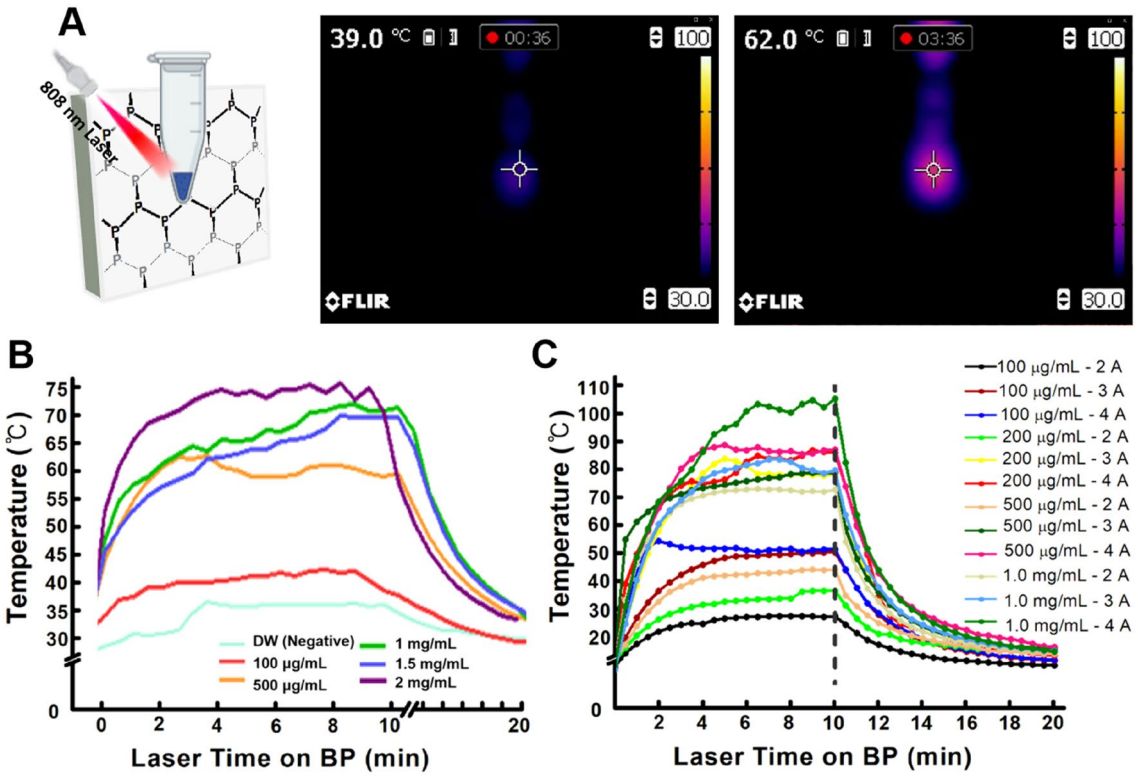

Fig. 3 Laser (808 nm)-plasmonic thermal effect of black phosphorous (BP). **A** Scheme of the 808 nm laser irradiation on BP. Thermographic images of the laser current – 3A on 100 μg/mL BP nanosheet samples at 36 s and 3 min 36 s. **B** Timeline of the laser-plasmonic thermal performances of BP nanosheets (500 μL, with different concentrations, irradiation with a current of – 2A for 10 min). C Irradiation current effects on the laser-plasmonic thermal performances of BP nanosheets (200 μL, within different concentrations)

under the BP concentration of 1000 μg/mL, in 4A reaction conditions, it could reach about 95 °C in 5 min, which was the melting temperature of DNA in the DNA extraction system. Meanwhile, it could reach 65 °C after 1 min after stopping laser irradiation, which would fit the temperature of DNA extraction. Hopefully, the controllable thermal system could lay a foundation for the subsequent use of BP and laser irradiation systems to enhance DNA extraction efficiency.

3.2 DNA extraction by the Optimized BP-NIR-HI System

According to the thermal report shown in Fig. 3C, BP nanosheets were added to the *E. coli* sample, and the mixture was irradiated by the 808 nm laser within 3 A current intensity. The irradiation remained for 5 min and the temperature of the system was about 55–60 °C for 2–3 min. This was followed by the nucleic acid extraction steps, resulting in the relatively pure DNA solution finally being obtained.

To verify the DNA extraction efficiency of the method for pathogenic bacteria, we used the same concentration of *E. coli* samples (10^5 CFU) by using the BP-NIR-HI system and QIAGEN kit method to detect the DNA content. First, different concentrations of BP (200 μg/mL; 500 μg/mL) and HI (DMS, 20 μL, 50 μL, 10 mg/mL) were used as different reaction conditions to detect the effect on DNA content extraction, and the same concentration of *E. coli* samples was used as that used for the QIAGEN kit method. After the DNA sample obtained after extraction was amplified by real-time PCR, the test results of the Ct (Cycle threshold) value under different reaction conditions were obtained (Fig. 4A). The results showed that the Ct values in the four experimental groups that used the BP-NIR-HI system for DNA extraction were all lower than those of the DW (negative control group) and QIAGEN kit group. Meanwhile, the above-mentioned DNA samples were tested for the nanodrop nucleic acid content (Fig. 4B), which confirmed that the experimental groups of BP-NIR-HI were higher than those of the DW (Deionized Water) and QIAGEN kit groups. Moreover, the nucleic acid content of the BP500-HI50 group was about three times higher than that of the QIAGEN kit group, hence proving the good DNA extraction efficiency of the method due to BP-NIR-HI's equivalence to the traditional commercial QIAGEN kit. In addition, the BP-NIR-HI system did not require the use of thermal incubators and heave centrifuges in the process (summarized in the workflow).

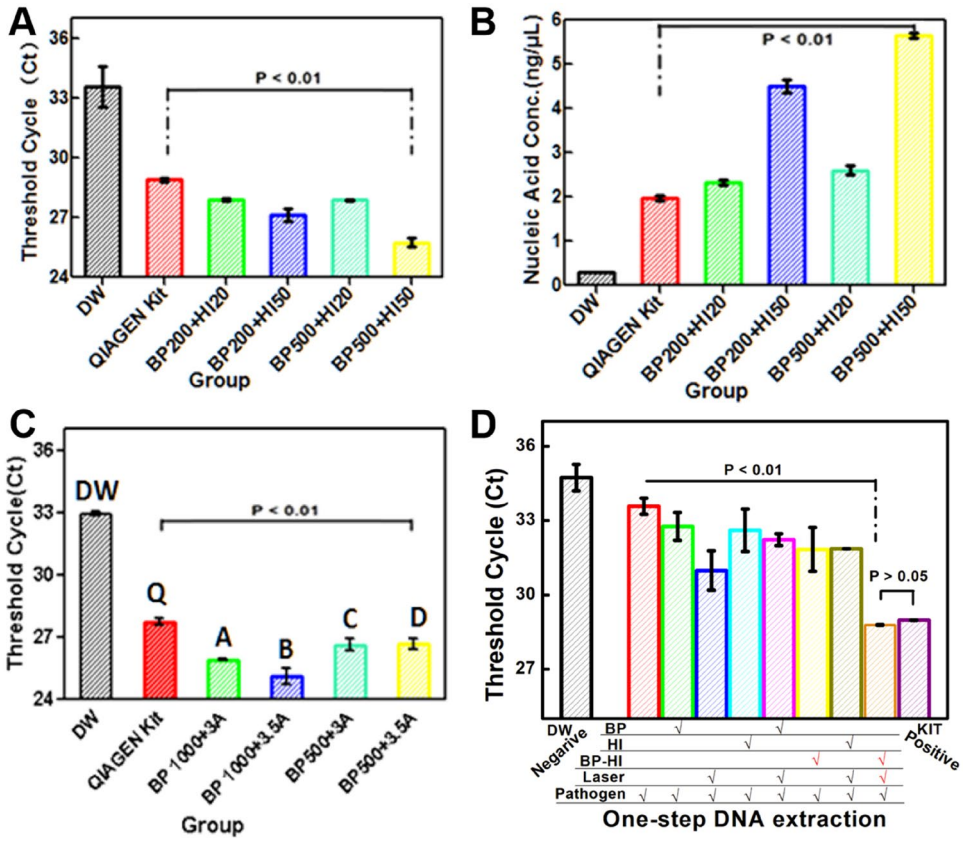

Fig. 4 Optimization of the black phosphorus-near infrared-homobifunctional imidoester (BP-NIR-HI) system. Comparison of real-time PCR results and nanodrop data of the BP-NIR-HI DNA extraction method. **A** Comparison of DNA amplification efficiencies with different ratios of BP and HI in the BP-NIR-HI system, experimental groups BP: 200 and 500 μg/mL, and HI: 20 and 50 μL. **B** Nucleic acid concentration of the extracted DNA through the BP-NIR-HI system. **C** Comparison of laser power for DNA extraction by the BP-NIR-HI system, experimental groups [different concentrations of BP (1000 and 500 μg/mL)] and different currents (3 and 3.5 A). **D** One-step BP-NIR-HI system design through the Ct value comparison of the BP-NIR-HI group with the single-factor group BP, HI, and laser and the double-factor group BP-HI, BP-laser, HI-laser, and control group DW and QIAGEN kit group after DNA amplification by real-time PCR

Furthermore, to explore the effects of different concentrations of BP and different currents on DNA extraction in the BP-NIR-HI system, the same concentration of *E. coli* (10^4 CFU) used 3 A and 3.5 A current intensity, and 1000 and 500 μg/mL BP were added to 50 μL of 10 mg/mL DMS, and DNA samples extracted from the DW group and QIAGEN kit group were compared at the same time. DNA amplification was also performed in the real-time PCR system (Fig. 4C). Results showed that the DNA content of the four experimental groups of BP-NIR-HI was higher than that of the QIAGEN kit and DW groups. At the same time, the extracted DNA content was under the influence of the 3.5 A current laser intensity, and 1000 μg/mL BP was the highest. On this basis, we carried out single factor (BP alone, HI alone, and laser irradiation alone), two-factor (BP-HI, BP-NIR laser, and HI-NIR laser), and three-factor (BP-NIR-HI) exploration of DNA extraction efficiency (Fig. 4D). Results demonstrated that DNA extraction could only be completed when BP, NIR laser, and HI acted simultaneously, and the Ct values of single- and dual-factor were all above 30, which proved that higher content of DNA could not be obtained, and there was no practical experimental significance. In summary, the concentration of BP, intensity of the laser current, and concentration of HI (DMS) all affected the extracted DNA content, because the current intensity and concentration of BP influenced the rising temperature of the reaction system. Moreover, HI affected the enrichment efficiency of DNA. Eventually, this led to differences in DNA content after extraction. DNA extraction can proceed normally and achieve the best extraction efficiency when all these three factors are involved.

3.3 Mechanism study of the BP-NIR-HI System for Nucleic Acid Extraction

For the study of the mechanism of DNA extraction of the BP-NIR-HI system, we explored the possible factors through

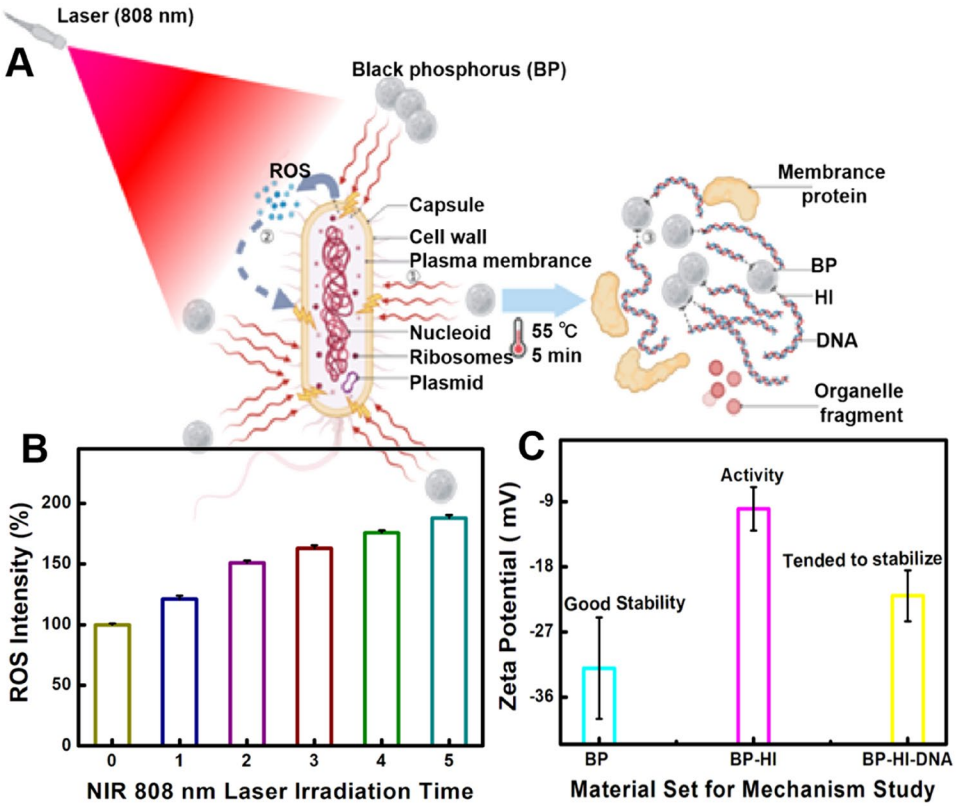

Fig. 5 Mechanism study of the black phosphorus-near infrared-homobifunctional imidoester (BP-NIR-HI) system. **A** Scheme of the bio-performances of BP under laser (NIR) plasmonic irradiation. **B** Reactive oxygen species (ROS) detection assay of BP with *E. coli*, Dichlorodihydrofluorescein diacetate (DCFAD) kit in 485/535 nm. **C** Stability study of the possible surface linking of DNA extraction between BP-HI and DNA

the qualitative method. Except for the obvious (a) thermal effect, which we have explained in the laser-plasmonic thermal performances of BP nanosheets [29, 30], the related chemical effects and the effective activity of BP nanosheets by HI crosslinking have been provided (Fig. 5A). (b) Studies have shown that BP causes an effective antioxidant to be present in the solution [27, 31, 32]. Here, we tested the intensity of the ROS of BP nanosheets by the dichlorodihydrofluorescein diacetate (DCFDA) ROS kit. We observed a sustaining ROS release from the degradation of DCFDA. Moreover, as we used longer irradiation, the amount of released ROS increased, which is a good sign that it helped the nucleic acid release in the system. We added 200 µL of BP nanosheets (500 µg/mL) to 200 µL of *E. coli* in a sample tube and used 3 A laser irradiation for different lengths of time (1–5 min). The OD (Optical Density) value of 560 nm was set for the detection. The experimental results are shown in Fig. 5B. With the gradual prolongation of irradiation time, the content of ROS production increased and reached about 192% of the blank control group at 5 min. Obviously, the production of a large amount of ROS is conducive to destroying the cell membrane, cytoplasm, and other components of the bacteria, as well as to the release of more DNA. (c) The principle of how HI works on biomaterial crosslinking has been studied for many applications [33, 34]. Here, we added the HI to activate the BP nanosheets and facilitate the linking of the nucleic acids to the surfaces of the BP nanosheets. In particular, we designed a study based on the processed composites during the extraction system where we used commercial chains of DNA to test whether the HI linked the BP and nucleic acids. The pure BP, BP-HI, and BP-HI-DNA were prepared by two dissolution methods. We found that the BP-HI composites showed some activity and the BP-HI-DNA showed mild stability (Fig. 5C) even after washing several times. We believe that this could be strong evidence for the crosslinking principle.

4 Conclusion

Here, we reported a new DNA extraction technology named the BP-NIR-HI system. The BP nanosheets have a series reaction in solution with NIR laser irradiation. The laser-plasmonic thermal performances of BP generated a high temperature after laser irradiation, which might cause the fragmentation of cell membranes and assist nucleic acid release. According to our characterization, we tested different concentrations of BP nanosheets for use with chemical lysis buffer for their ability to assist with nucleic acid release from cells. The current method of an NIR laser has been optimized through multi-point tests. HI, as the biocompatible cross-linking reagent, was added to the reaction to enrich and attract the nucleic acid to the BP nanosheets after thermal lysis. Moreover, the applied HI helped the nucleic

acid crosslink with BP nanosheets, and the eluted nucleic acid could be applied for further diagnosis. Furthermore, BP-NIR-HI system did not require the use of thermal incubators and heave centrifuges in the process Hopefully, studying the bio-applications of BP nanosheets will bring us further opportunities for clinical applications.

Author contributions JKK and YS supervised the project. YS, HL, QZ, and MGK conceived the research. YS, QZ, and HL designed the experiments. YS, QZ, HL, MK, ZQ, and YJ performed the analysis and interpreted the data. BK, MGK, and HL provided chemicals and supported data analysis. J-KK provided comments and suggested appropriate modifications. YS, HL, QZ, and YS wrote and edited the manuscript. All authors read and approved the final manuscript.

Funding This work was supported by the Yonsei University Research Fund of 2021–22-005, Republic of Korea, and also supported by the National Research Foundation of Korea (NRF) (2019R1A2C2084122), Republic of Korea.

Declarations

Conflicts of interest The authors declare no Conflicts of interests/Competing interests.

References

1. Kurozumi, S., Yamaguchi, Y., Kurosumi, M., Ohira, M., Matsumoto, H., Horiguchi, J.: Recent trends in microRNA research into breast cancer with particular focus on the associations between microRNAs and intrinsic subtypes. J. Hum. Genet. **62**(1), 15–24 (2017)
2. Huang, H.S., Tsai, C.L., Chang, J., Hsu, T.C., Lin, S., Lee, C.C.: Multiplex PCR system for the rapid diagnosis of respiratory virus infection: systematic review and meta-analysis. Clin. Microbiol. Infect. **24**(10), 1055–1063 (2018)
3. Qiao, Z., Seo, H., Liu, H., Cha, H.H., Kim, J.Y., Kim, S.H., et al.: Simple and sensitive diagnosis of invasive aspergillosis using triphasic DE−ZnO−APDMS microparticle composite. Sens. Actuators B Chem. **346**, 130487 (2021)
4. Qian, Y., Yuan, W.E., Cheng, Y., Yang, Y., Qu, X., Fan, C.: Concentrically integrative bioassembly of a three-dimensional black phosphorus nanoscaffold for restoring neurogenesis, angiogenesis, and immune homeostasis. Nano Lett. **19**(12), 8990–9001 (2019)
5. Kim, S.M., Kim, J., Noh, S., Sohn, H., Lee, T.: Recent development of aptasensor for influenza virus detection. Biochip J. **14**, 1–13 (2020)
6. Kim, S., Lee, J., Koo, B., Kwon, D., Jeon, S., Shin, Y., et al.: Floating magnetic membrane for rapid enrichment of pathogenic bacteria. BioChip J. **15**(1), 61–68 (2021)
7. Huang, C., Hu, S., Zhang, X., Cui, H., Wu, L., Yang, N., et al.: Sensitive and selective ctDNA detection based on functionalized black phosphorus nanosheets. Biosens. Bioelectron. **165**, 112384 (2020)
8. Liu, Q., Fan, T., Zheng, Y., Yang, S.-l, Yu, Z., Duo, Y., et al.: Immunogenic exosome-encapsulated black phosphorus nanoparticles as an effective anticancer photo-nanovaccine. Nanoscale **12**(38), 19939–19952 (2020)
9. Nijhuis, R., Guerendiain, D., Claas, E., Templeton, K.: Comparison of ePlex respiratory pathogen panel with laboratory-developed real-time PCR assays for detection of respiratory pathogens. J. Clin. Microbiol. **55**(6), 1938–1945 (2017)
10. Lee, W.S., Ahn, J., Jung, S., Lee, J., Kang, T., Jeong, J.: Biomimetic nanopillar-based biosensor for label-free detection of influenza A virus. Biochip J. **15**, 1–8 (2021)
11. Kim, J., Hwang, E.-S.: Multiplexed diagnosis of four serotypes of dengue virus by real-time RT-PCR. BioChip J. **14**(4), 421–428 (2020)
12. Jang, Y.O., Lee, H.J., Koo, B., Cha, H.H., Kwon, J.-S., Kim, J.Y., et al.: Rapid COVID-19 molecular diagnostic system using virus enrichment platform. Biosensors **11**(10), 373 (2021)
13. Katevatis, C., Fan, A., Klapperich, C.M.: Low concentration DNA extraction and recovery using a silica solid phase. PLoS One **12**(5), e0176848 (2017)
14. Kim, S., Lee, J., Koo, B., Kwon, D., Jeon, S., Shin, Y., Joo, J.: Floating magnetic membrane for rapid enrichment of pathogen bacterial. BioChip J. **15**, 61–68 (2021)
15. Liu, H., Dao, T.N.T., Koo, B., Jang, Y.O., Shin, Y.: Trends and challenges of nanotechnology in self-test at home. TrAC Trends Anal. Chem. **144**, 116438 (2021)
16. Petralia, S., Barbuzzi, T., Ventimiglia, G.: Polymerase chain reaction efficiency improved by water soluble β-cyclodextrins capped platinum nanoparticles. Mater. Sci. Eng., C **32**(4), 848–850 (2012)
17. Zhao, F., Koo, B., Liu, H., Jin, C.E., Shin, Y.: A single-tube approach for in vitro diagnostics using diatomaceous earth and optical sensor. Biosens. Bioelectron. **99**, 443–449 (2018)
18. Liu, H., Zhao, F., Koo, B., Luan, Y., Zhong, L., Yun, K., et al.: Dimethyl 3, 3′-dithiobispropionimidate (DTBP) as a cleavable disulfide-based polymer to encapsulate nucleic acids in biological sample preparation. Sens. Actuators B Chem. **288**, 225–231 (2019)
19. Qiao, Z., Liu, H., Noh, G.S., Koo, B., Zou, Q., Yun, K., et al.: A simple and rapid fungal DNA isolation assay based on ZnO nanoparticles for the diagnosis of invasive aspergillosis. Micromachines. **11**(5), 515 (2020)
20. Barman, S.C., Sharifuzzaman, M., Zahed, M.A., Park, C., Yoon, S.H., Zhang, S., et al.: A highly selective and stable cationic polyelectrolyte encapsulated black phosphorene based impedimetric immunosensor for Interleukin-6 biomarker detection. Biosens. Bioelectron. **186**, 113287 (2021)
21. Qiao, P., Wang, X.H., Gao, S., Yin, X., Wang, Y., Wang, P.: Integration of black phosphorus and hollow-core anti-resonant fiber enables two-order magnitude enhancement of sensitivity for bisphenol A detection. Biosens. Bioelectron. **149**, 111821 (2020)
22. Kang, J.S., Ke, M., Hu, Y.: Ionic intercalation in two-dimensional van der Waals materials: in situ characterization and electrochemical control of the anisotropic thermal conductivity of black phosphorus. Nano Lett. **17**(3), 1431–1438 (2017)
23. Antonatos, N., Bousa, D., Kovalska, E., Sedmidubsky, D., Ruzicka, K., Vrbka, P., et al.: Large-scale production of nanocrystalline black phosphorus ceramics. ACS Appl. Mater. Interfaces. **12**(6), 7381–7391 (2020)
24. Lee, H.U., Lee, S.C., Won, J., Son, B.-C., Choi, S., Kim, Y., et al.: Stable semiconductor black phosphorus (BP)@titanium dioxide (TiO2) hybrid photocatalysts. Sci. Rep. **5**(1), 1–6 (2015)
25. Qu, G., Xia, T., Zhou, W., Zhang, X., Zhang, H., Hu, L., et al.: Property–activity relationship of black phosphorus at the nano–bio interface: from molecules to organisms. Chem. Rev. **120**(4), 2288–2346 (2020)
26. Lee, J.Y., Lin, Y.J.: Effect of incorporation of black phosphorus into PEDOT: PSS on conductivity and electron–phonon coupling. Synth. Met. **212**, 180–185 (2016)
27. Liu, H., Zhao, F., Jin, C.E., Koo, B., Lee, E.Y., Zhong, L., et al.: Large instrument-and detergent-free assay for ultrasensitive nucleic acids isolation via binary nanomaterial. Anal. Chem. **90**(8), 5108–5115 (2018)

28. Wu, S., Hui, K.S., Hui, K.N.: 2D black phosphorus: from preparation to applications for electrochemical energy storage. Adv. Sci. **5**(5), 1700491 (2018)
29. He, D., Wang, Y., Huang, Y., Shi, Y., Wang, X., Duan, X.: High-performance black phosphorus field-effect transistors with long-term air stability. Nano Lett. **19**(1), 331–337 (2018)
30. Zhou, L., Liu, C., Sun, Z., Mao, H., Zhang, L., Yu, X., et al.: Black phosphorus based fiber optic biosensor for ultrasensitive cancer diagnosis. Biosens. Bioelectron. **137**, 140–147 (2019)
31. Kong, N., Ji, X., Wang, J., Sun, X., Chen, G., Fan, T., et al.: ROS-mediated selective killing effect of black phosphorus: mechanistic understanding and its guidance for safe biomedical applications. Nano Lett. **20**(5), 3943–3955 (2020)
32. Jiang, X., Jin, H., Gui, R.: Visual bio-detection and versatile bio-imaging of zinc-ion-coordinated black phosphorus quantum dots with improved stability and bright fluorescence. Biosens. Bioelectron. **165**, 112390 (2020)
33. Liu, H., Noh, G.S., Luan, Y., Qiao, Z., Koo, B., Jang, Y.O., et al.: A sample preparation technique using biocompatible composites for biomedical applications. Molecules **24**(7), 1321 (2019)
34. Lee, E.Y., Kim, Y., Koo, B., Noh, G.S., Lee, H., Shin, Y.: A novel nucleic acid amplification system based on nano-gap embedded active disk resonators. Sens. Actuators B Chem. **320**, 127351 (2020)